Rapid translocation of NGR proteins drives polarization of PIN-activating D6 protein kinase during root gravitropism

Ivan Kulich*, Julia Schmid*, Anastasia Teplova*, Linlin Qi, Jiří Friml

Institute of Science and Technology Austria (ISTA), Klosterneuburg, Austria

* These authors contributed equally and are listed alphabetically.

e-mail: jiri.friml@ist.ac.at

Abstract

Root gravitropic bending represents a fundamental aspect of terrestrial plant physiology. Gravity is perceived by sedimentation of starch-rich plastids (statoliths) to the bottom of the central root cap cells. Following gravity perception, intercellular auxin transport is redirected downwards leading to an asymmetric auxin accumulation at the lower root side causing inhibition of cell expansion, ultimately resulting in downwards bending. How gravity-induced statoliths repositioning is translated into asymmetric auxin distribution remains unclear despite PIN auxin efflux carriers and the Negative Gravitropic Response of roots (NGR) proteins polarize along statolith sedimentation, thus providing a plausible mechanism for auxin flow redirection. In this study, using a functional NGR1-GFP construct, we visualized the NGR1 localization on the statolith surface and plasma membrane (PM) domains in close proximity to the statoliths, correlating with their movements. We determined that NGR1 binding to these PM domains is indispensable for NGR1 functionality and relies on cysteine acylation and adjacent polybasic regions as well as on lipid and sterol PM composition. Detailed timing of the early events following graviperception suggested that both NGR1 repolarization and initial auxin asymmetry precede the visible PIN3 polarization. This discrepancy motivated us to unveil a rapid, NGR-dependent translocation of PIN-activating AGCVIII kinase D6PK towards lower PMs of gravity-perceiving cells, thus providing an attractive model for rapid redirection of auxin fluxes following gravistimulation.

Introduction

Plants are capable of sensing gravity and adjust their organs' growth direction accordingly. This phenomenon is called gravitropism, with positive gravitropism referring to the root growing down towards the Earth center and negative gravitropism describing the upward growth of the shoot (Kawamoto and Morita, 2022; Kolesnikov et al., 2016; Takahashi et al., 2021). The model plant *Arabidopsis thaliana* senses gravity in central

root cap (columella) cells and the shoot endodermal cells and, in special gravity-sensing cells, which contain starch-enriched plastids – amyloplasts (Kiss et al., 1997, 1996, 1989; Morita, 2010). Due to their higher density, amyloplasts thus act as statoliths and sediment within cells (Sack, 1991). Following amyloplast sedimentation, the PIN exporters for the plant hormone auxin (PIN3 and PIN7) polarize towards the bottom cell sides, thus creating a downwards polarized auxin flow, which correlates with the asymmetric auxin accumulation at the lower side of the organ mediating the shoot/root curvature (Friml et al., 2002; Kleine-Vehn et al., 2010; Rakusová et al., 2011; Band et al., 2012). While sedimenting amyloplasts clearly serve as a signal for asymmetric auxin distribution, the precise mechanism remains elusive (Han et al., 2021; Kiss et al., 1989).

Recently, the LAZY protein family has been identified as a crucial player in the process of auxin redistribution and normal tropic response for both roots and shoots following gravistimulation (Jiao et al., 2021; Li et al., 2007; Yoshihara et al., 2013; Yoshihara and Iino, 2007). LZY1, LZY2, and LZY3 function redundantly in shoot gravitropism; LZY2, LZY3, and LZY4 - also referred to as NGR1, NGR3, and NGR2 (NEGATIVE GRAVITROPIC RESPONSE OF ROOTS) - regulate the root gravitropism (Kawamoto and Morita, 2022). *ngr1,2,3* triple mutant plants display an anti-gravitropic phenotype with the root growing slightly upwards (Ge and Chen, 2016). This phenotype is accompanied by an inverted PIN3 polarization, thus redirecting the auxin flow to the upper side of the gravistimulated root (Ge and Chen, 2019; Taniguchi et al., 2017). Additionally, it was recently demonstrated that following gravistimulation, NGR3 localizes asymmetrically to the plasma membrane (PM) in columella cells of lateral roots (Furutani et al., 2020). However, the structure and molecular function of NGR proteins, as well as specific domains that could allow for PM association and polarization are still unknown. Polarization of NGR3 further acts as a precursor of PIN3 relocalization (Furutani et al., 2020). Additionally, PIN transport activity is fine-tuned by phosphorylation mediated by AGCVIII serine/threonine kinases like D6 PROTEIN KINASE (D6PK) (Barbosa and Schwechheimer, 2014). Whether additional factors play a role in this signaling cascade and how the underlying molecular mechanism connecting gravity sensing to asymmetric auxin distribution may look like, remains to be investigated.

Here, we provide novel insights into mechanisms of gravity-induced NGR1 polarization and downstream processes leading to PIN-dependent auxin fluxes activation and ultimately, gravitropic bending. We show the crucial function of polybasic regions and acylation of NGR1 for its binding to the PM and amyloplasts in columella cells, which is essential for its function in gravitropic bending. Pharmacological approaches show that the membrane composition affects NGR1 PM binding and polarization. Finally, we show

rapid translocation of PIN activator – D6 protein kinase as an event downstream of NGR signaling. These observations suggest a model where statolith sedimentation is accompanied by rapid NGR relocation, which mediates similar relocation of the D6PK activator of PIN transporters, providing means to rapidly redirect asymmetric auxin fluxes in response to gravity.

Results

NGR1 localizes to statoliths and their sedimentation is accompanied by NGR1 polarization at the lower PM

To observe NGR localization in the columella cells, we cloned *NGR1-GFP* under its native promoter (*NGR1p::NGR1-GFP*) and transformed it into the *ngr1/2/3* triple mutants. This construct fully rescued the agravitropic bending phenotype of the *ngr1/2/3* triple mutant (see further), proving functionality of the GFP-tagged protein. NGR1-GFP displayed a highly specific columella expression, which was most prominent at the PM and the statolith periphery. NGR1-GFP signal from the PM was not evenly distributed, but rather polarized to the lower side of the columella cells in the vicinity of the sedimented statoliths (Fig. 1A).

Constitutive overexpression of NGR1-GFP under 35S promoter (*35Sp::NGR1-GFP*) confirmed that in multiple other cell types, NGR1-GFP localizes to the PM suggesting direct membrane binding mechanism. Additionally, NGR1 is associated with other plastid types such as chloroplasts in guard cells (Fig. S1A). To separate the GFP signal from the chlorophyll, we used fluorescence lifetime imaging, which confirmed that NGR1-GFP localizes at the chloroplast periphery (Fig. S1B). This implies a general plastid targeting mechanism of NGR. Notably, chloroplasts in the vicinity of the PM strongly correlated with NGR1 accumulating at the PM nearby, similar to the scenario in columella (Fig. S1A,C).

This shows that NGR1-GFP localizes to the plastids and PM in their vicinity providing a mechanism for how gravity-induced statolith sedimentation can polarize NGR1-GFP to the bottom PM.

Timing of events during the gravitropic response

Next, we tracked the timing of events during gravitropic bending. For that, we used a vertical stage microscope with a rotation stage allowing us to perform gravistimulation while imaging and minimize the time required for rotating the sample. For the gravistimulation, roots, initially located vertically, were rotated 90° from the vertical position (located horizontally). Further gravistimulation was performed by flipping the root

180° (with the root tip from pointing left to pointing right, or vice versa). 180° rotations were performed during the imaging thus the precise timing could be determined from the individual frame timestamps. Following gravitropic stimulus, NGR1 at the PM relocalized dynamically with the falling statoliths (Fig. 1B). First, the signal at the top membrane decreased and then reached the bottom PM together with statoliths, around 5 minutes after the stimulation (Fig. 1C,D). If the root was rotated 180° from the vertical position (from root tip pointing down to pointing up), the time required for the statolith sedimentation has increased due to the cell's elongated shape and the presence of vacuole. In such a scenario, it took more than 15 minutes for the statoliths to fall. Again, the increase of the NGR1 signal at the bottom side correlated with the statolith occurrence, implying that statolith vicinity is the region where NGR1 signal gets enriched (Fig. S1D). When monitored for an extended period of time, NGR1 signal was always decorating the PM proximal to the statolith (Supplementary movie 1).

To put these early gravitropic events in the context of the auxin gradient formation, we tracked PIN3 localization dynamics, intracellular calcium transients, and auxin reporter DII-Venus (Brunoud et al., 2012). Calcium transients are one of the fastest known auxin response events (Monshausen et al., 2011) and we monitored them using plants stably transformed with GCaMP3 fluorescent sensor (Zariwala et al., 2012). While the signal increase at the bottom side of the root was visible within a minute after statoliths touched the bottom membrane, its decrease at the top PM started immediately after rotation. This implies that the first signaling event in the root gravitropic bending is the statolith removal from the top membrane, rather than its arrival at the bottom (Fig. 1E). While subsequent changes in the DII-Venus degradation were consistent with the calcium-based timing, the first visible PIN3 polarization to the bottom columella cell sides was detectable only after 15 minutes (Fig. 1F,G). Nonetheless, already the earliest auxin asymmetry is likely generated by PIN-mediated polar auxin transport as it was completely blocked by the treatment with N-1-naphthylphthalamic acid (NPA) (Fig. 1E), a PIN inhibitor (Abas et al., 2021).

To summarize, statolith sedimentation is accompanied by rapid NGR1 relocation to the PM subdomain proximal to the NGR1-containing statoliths. The first event in gravitropic response is the NGR1 leaving the top membrane accompanied by decrease in the auxin signaling at the upper root side, followed by NGR1 arrival at the bottom membrane and increase in auxin signaling at the bottom side. This initial auxin asymmetry is mediated by PIN-dependent auxin transport, despite visible polarization of PIN3 can be detected only later.

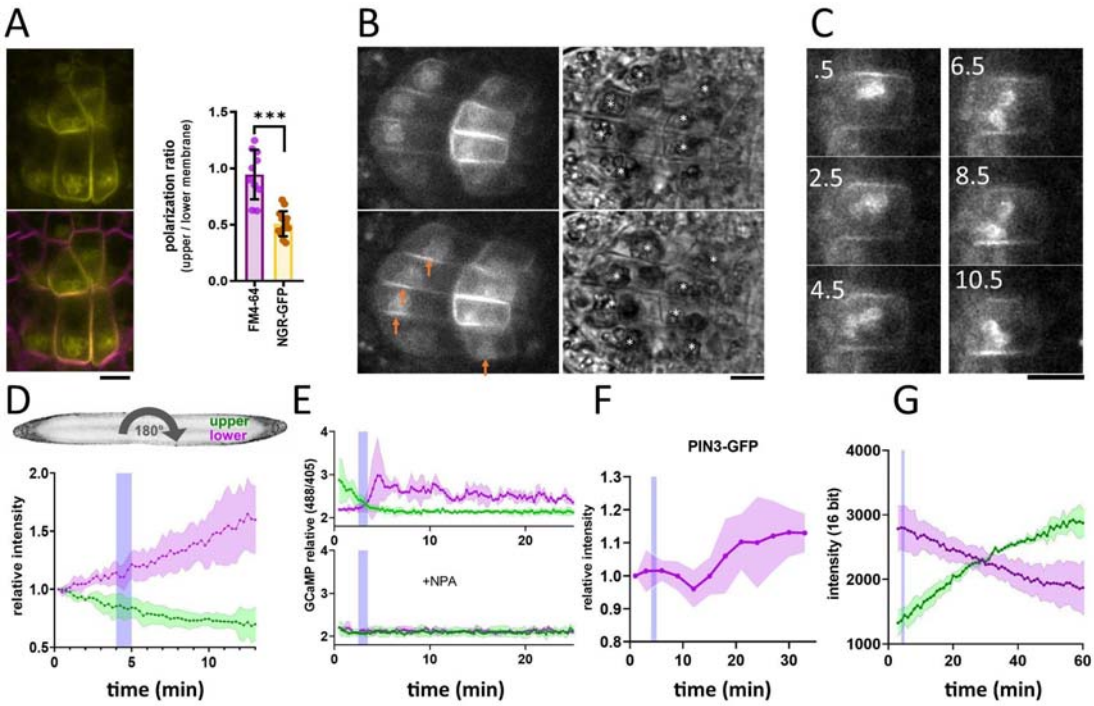

Fig. 1 | NGR1-GFP relocalization in the root columella.

A) Colocalization of NGR1-GFP (yellow) with membrane stain FM4-64 (magenta). The statolith periphery is also decorated by the NGR1-GFP signal. NGR1-GFP is significantly polarized to the bottom area as quantified using upper/lower signal ratio (1 = even distribution)

B) NGR1-GFP ~30 seconds and 5 minutes after gravitropic bending. Orange arrows depict areas where the signal increased after contact with the statoliths. White stars in the transmission channel depict statoliths.

C) Time course of individual columella cell expressing NGR1-GFP. Numbers depict minutes from the 180° rotation.

D) Top: schematic depiction of the experiment design (valid for D-G). Bottom: Quantification of the NGR1-GFP signal at the lower and upper membranes. Similar setup was used for E. and F. Blue stripes in D-F represent intervals at which statoliths touched the bottom membrane. Average of 5 biological replicas. Shaded regions depict standard deviation (SD).

E) GCaMP signal after root gravitropic bending without (top) and with 20µM NPA (bottom). The data represent 3 technical replicates, and 3 additional biological replicates were conducted, yielding similar results. Shaded regions depict SD.

F) PIN3 enrichment at the bottom of the central columella cells. The average is based on data from 5 biological replicas. Shaded regions depict SD.

G) DII Venus signal changes after root gravitropic bending. The average is calculated from 3 biological replicas. Shaded regions depict SD.

Blue lines represent approximate time of statolith contact with the new bottom membrane. Bars = 10 µm

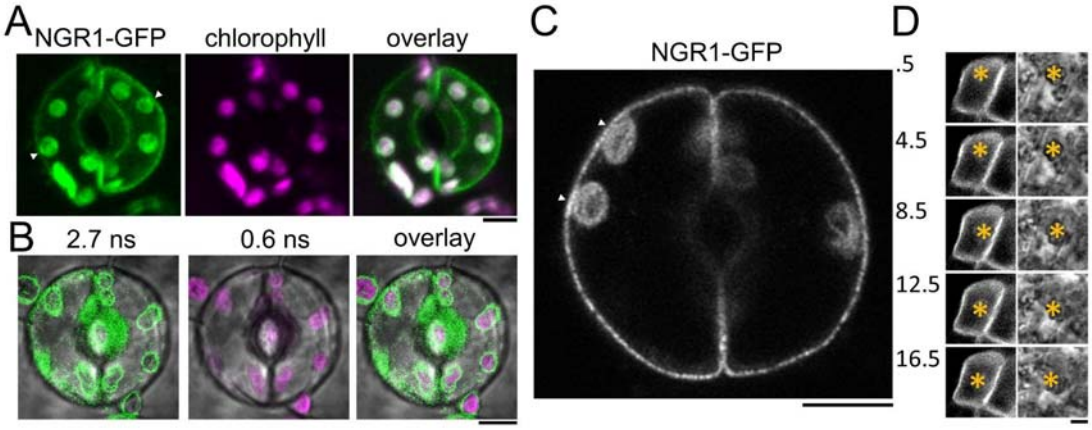

Fig. S1 | NGR1 localization in columella and guard cells.

A) 35Sp::NGR1-GFP colocalization with chloroplasts in guard cells. Contact sites with PM are depicted by white arrowheads.

B) 35Sp::NGR1-GFP colocalization with chloroplasts in guard cells performed by fluorescence lifetime imaging to separate chlorophyll autofluorescence from GFP.

C) 35Sp::NGR1-GFP in guard cells imaged using airyscan superresolution. White arrowheads point to areas of contact with the PM.

D) NGR1p::NGR1-GFP localization in the columella cell rotated from vertical position upside down (180°). Numbers indicate minutes after rotation.

Bars = 5 µm

NGR1 polarization does not require BFA-sensitive trafficking

To gain more insight into the dynamics of the NGR1 localization to the PM and amyloplasts, we tested different inhibitors to alter membrane composition and interfere with endocytic trafficking. Recently, it has been shown that RCC1-like domain (RLD) proteins directly interact with NGRs and play a crucial role in polar auxin transport during gravity signaling (Furutani et al., 2020). As RLD trafficking is known to be sensitive to the ARF-GEF inhibitor Brefeldin A (BFA) (Furutani et al., 2020; Wang et al., 2022), we examined if the drug also affects the localization and polarization of NGR1. 5-day-old *NGR1p::NGR1-GFP* seedlings were incubated with 50 µM BFA together with the protein synthesis inhibitor, cycloheximide (CHX, 50 µM) and the endocytic tracer FM4-64 (2 µM)

as described previously (Geldner et al., 2001). Interestingly, while FM4-64-stained membranes accumulated into so-called BFA compartments, NGR1-GFP did not and still showed association with the PM and amyloplasts (Fig. 2A-C). Furthermore, the polarization of NGR1 following gravity stimulation was not disrupted in the presence of BFA. Similar effects were observed in overexpressed NGR1 as it also did not show co-localization with BFA aggregates (Supplementary Fig. 2A-C).

This shows that NGR1 localization and gravity-induced polarization does not undergo BFA-sensitive endocytic recycling mediated by the ARF-GEF GNOM as it has been shown for other proteins involved in gravity response like RLDs and PINs (Geldner et al., 2001; Naramoto et al., 2014; Wang et al., 2022).

NGR1 PM association requires specific membrane composition

NGR1 displays PM localization although transmembrane domains are not predicted in its structure and it does not undergo BFA-sensitive trafficking. This implies the existence of posttranslational modifications such as S-acylation or N-myristoylation to associate with PM. For initial insight we used GPS Lipid prediction tool (Xie et al., 2016), which navigated us towards S-acylation. To test for the presence of S-acylation sites, we utilized the reducing properties of Dithiothreitol (DTT), which interferes with the formation of the thioester bond thus effectively preventing S-acylation (Sabol et al., 2017). Following previously described conditions, NGR1-GFP showed an increase in cytoplasmic signal and reduction of PM association (Fig. 2D). Similar effect of DTT was observed when expressing NGR1 under the 35S promoter, suggesting that there is indeed an acylation site (Fig. S2D-E). Interestingly, NGR1 still localizes to amyloplasts, indicating a different way of plastid association compared to the PM.

Next, we tested whether apart from the NGR1 S-acylation, the membrane composition itself might be essential for the NGR1 PM association. Previously it has been shown that polybasic regions (PBRs) of proteins can target them to anionic phospholipids like PtdIns(4)P (PI4P) (Hammond et al., 2012; McLaughlin and Murray, 2005). We tested whether the depletion of PI4P from the PM will affect the NGR1 PM association. *NGR1p::NGR1-GFP* seedlings were incubated for 30 minutes with 30 µM phenylarsine oxide (PAO), a PtdIns(4)-kinase inhibitor (Hammond et al., 2012; Vermeer et al., 2009). The NGR1-GFP cytosolic signal was significantly increased, indicating that the interplay between PBRs and phospholipids is important for NGR1 PM but not amyloplast association (Fig. 2D).

Next, we wanted to determine whether sterols might influence the PM association of NGR1. *NGR1-GFP* seedlings were grown on fenpropimorph (FEN), an inhibitor of sterol

biosynthesis that decreases the number of sterols and can trigger their conversion into cyclopropyl sterols (Frescatada-Rosa et al., 2014). NGR1-GFP showed an increase in cytoplasmic signal and membrane localization was largely lost (Fig. 2D). Comparable effects were also observed after treatment with another sterol synthesis inhibitor lovastatin (LOV) (Fig. 2D; Fig. S2F). However, similarly to DTT and PAO, amyloplast localization could not be disturbed.

These observations show that NGR1 PM but not necessarily plastid localization depends likely on acylation, phospholipid, and sterol membrane composition.

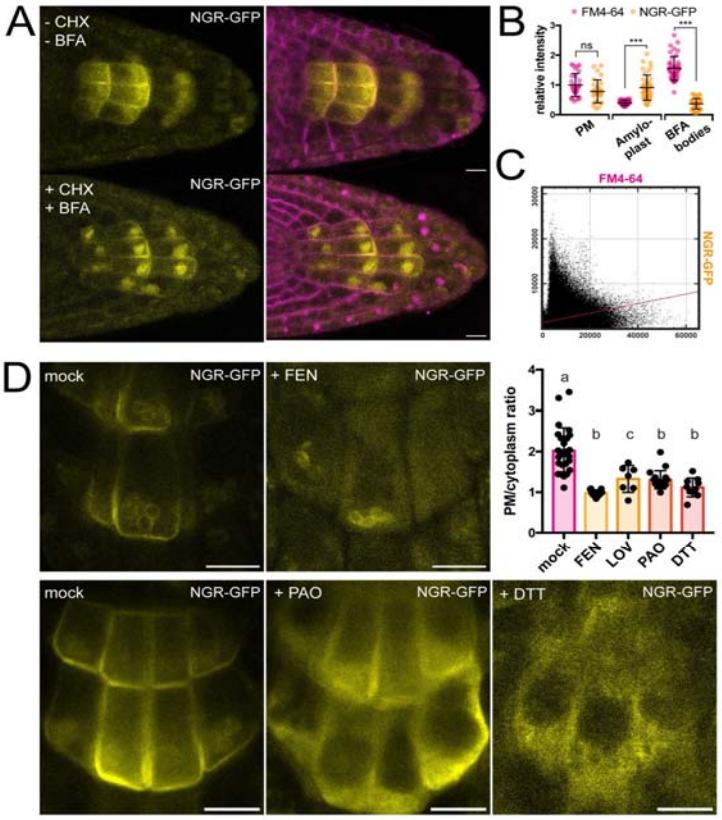

Fig. 2 | Role of trafficking and PM composition in NGR1 localization.

A) Representative images of *NGR1p::NGR1-GFP* roots treated with 50 µM CHX, 50 µM BFA, and 2 µM FM4-64; mock: DMSO; NGR1-GFP in yellow, FM4-64 in magenta. 3 biological replicas were made with similar results. Error bars represent SD.

B) Fluorescence intensity of FM4-64 and NGR1-GFP at the PM (n = 29), amyloplasts (n = 39) and BFA bodies (n = 42) normalized to the average fluorescence intensity of FM4-64 at the PM. Data is pooled from columella cells of the representative experiment shown in Fig. 2A. *n* equals measured points. Statistical measurements were done with one-way ANOVA; *** equals adj. p-value of <0.0001.

C) Cytofluorogram of colocalization of FM4-64 and NGR1-GFP from the figure 2A using Pearson's coefficient.

D) *NGR1p::NGR1-GFP* roots treated with FEN, PAO, and DTT. PM/cytoplasm ratio was calculated for mock (n = 26), FEN (n = 11), LOV (n = 7), PAO (n = 18), and DTT (n = 10) treated seedlings. *n* equals the number of cells evaluated. Using one-way ANOVA, *b* is significantly different from *a* with an adj. p-value of <0.0001, *c* is significantly different from *a* with an adj. p-value of 0.006.

Bars = 10 µm

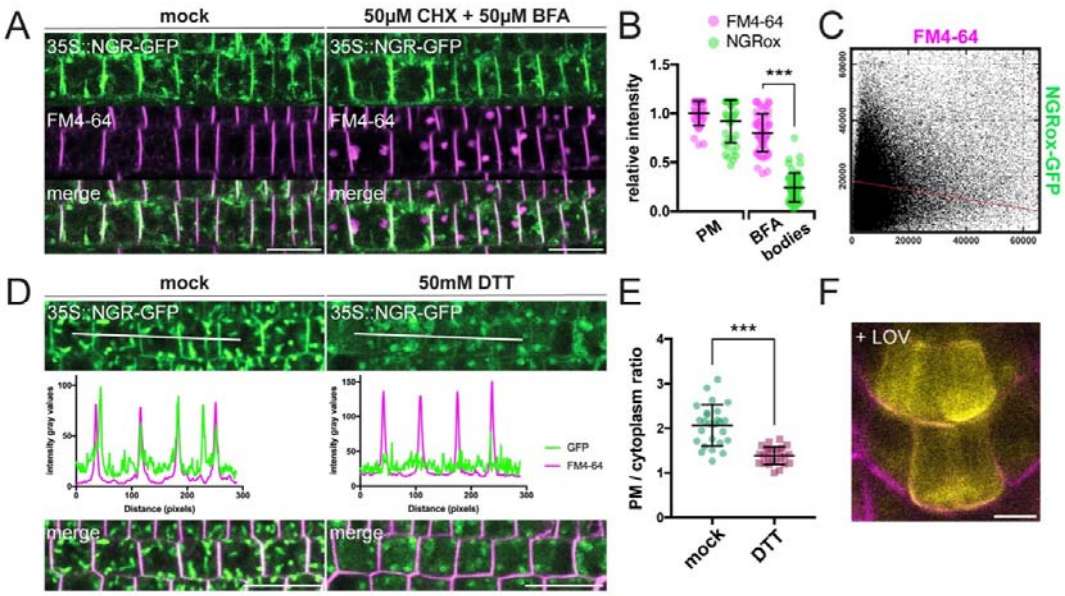

Fig. S2 | Pharmacological treatments of *35Sp::NGR1-GFP* seedlings.

A) Representative images of BFA treated *35Sp::NGR1-GFP* seedlings: pretreatment with 50 µM CHX, followed by treatment with 50 µM BFA for 90 min and 2 µM FM4-64 for 10 min. mock: DMSO. 3 additional biological replicas were made with similar results. Bars = 20µm

B) BFA treatment of *35Sp::NGR1-GFP* seedlings: fluorescence intensity of FM4-64 and 35Sp::NGR1-GFP at PM (n = 40) and BFA bodies (n = 54) normalized to average intensity of FM4-64 at the PM (=1); statistical analysis with one-way ANOVA: *** equals p-value <0.0001

C) Cytofluorogram of JACoP colocalization analysis; intensity of pixels of FM4-64 on x-axis and 35Sp::NGR1-GFP on y-axis. Data is derived from the experiment shown in Fig. S2A.

D) 50 mM DTT treatment of *35Sp::NGR1-GFP* plants for 3 h followed by 10 min co-treatment with 2 µM FM4-64; intensity profile measured along white line. 3 additional biological replicas were made with similar results. Bars = 20µm

E) PM/cytoplasm signal ratio for untreated (n = 26) and 50 mM DTT treated (n = 25) *35Sp::NGR1-GFP* seedlings; *n* represents number of cells evaluated. Statistical analysis with unpaired t-test; *** equals p-value <0.0001

F) Representative image of 1 µM LOV treated *NGR1p::NGR1-GFP* seedlings; NGR1p::NGR1-GFP in yellow, FM4-64 in magenta. Bars = 10µm

NGR1 PM localization is synergistically mediated by polybasic regions and a palmitoylation site

To further study NGR1 membrane localization, we examined the amino acid sequence of the NGR1 to understand which sites of the protein mediate its association with the membrane. We noticed 2 polybasic regions $K^{113}K^{114}R^{115}K^{116}$ (PBR1) and $K^{186}K^{187}K^{188}R^{189}$ (PBR2) – these strands of positively charged amino acids may mediate the interaction of NGR1 with negatively charged phospholipids. Also, we noticed a conserved Cys^{206} residue – a potential S-palmitoylation (PALM) site according to the GPS-Lipid post-translational modification prediction tool (Xie et al., 2016).

To test the role of these sites in the NGR1 membrane localization we performed site-directed mutagenesis based on the *NGR1p::NGR1-GFP* construct. We introduced mutations $K^{114}E\&R^{115}E$ (-PBR1), and $K^{187}E\&K^{188}E$ (-PBR2) to the polybasic regions of the NGR1 to neutralize their positive charge, and mutated the conserved cysteine $C^{206}A$ (-PALM) to abolish the potential palmitoylation site (Fig. 3A). *NGR1^{-PALM}-GFP*, *NGR1^{-PBR2}-GFP*, and *NGR1$^{-PBR1\&2}$-GFP* under the native *NGR1* promoter were transformed into the *ngr1/2/3* background. These mutant versions of the *NGR1* restored the anti-gravitropic root phenotype of the *ngr1/2/3* triple mutant similar to the *NGR1-GFP* version without mutations (Fig. S3A). The *NGR1^{-PALM}* version resembled the root bending of the *NGR1^{WT}-GFP* version, and *NGR1^{-PBR2}* and *NGR1$^{-PBR1\&2}$* versions demonstrated a slight delay in the main root angle restoration after reorientation in the vertical scanner setup (Fig. S3B). Then we performed confocal imaging of the root columella cells to check the localization of the NGR1^{-PALM}-GFP, NGR1^{-PBR2}-GFP, and NGR1$^{-PBR1\&2}$-GFP proteins (Fig. S3C). To compare the different mutant versions, we quantified the PM/cytoplasm signal ratio. The PM/cytoplasm ratio was slightly decreased for NGR1^{-PALM}-GFP, NGR1^{-PBR2}-GFP, and NGR1$^{-PBR1\&2}$-GFP mutants compared to NGR1^{WT}-GFP (Fig. S3D).

As the mutations only in the palmitoylation site or only in the polybasic regions of the NGR1 did not lead to the significant disruption of the plant gravitropic response and the

dissociation of the protein from the membrane, we combined these mutations to check their collective effect. We generated NGR1$^{-PALM\&PBR2}$-GFP with a mutation in the PALM site and the PBR2, and NGR1$^{-PALM\&PBR1\&2}$ with a mutation in both PBR1 and PBR2 and PALM site. *NGR1p::NGR1$^{-PALM\&PBR2}$-GFP* and *NGR1p::NGR1$^{-PALM\&PBR1\&2}$-GFP* could not fully complement *ngr1/2/3* triple mutant. The main root of the 5 d.o. seedlings demonstrated inclination from the vertical angle (Fig. S3E). In contrast to *NGR1-GFP* complemented *ngr1/2/3* plants, complementation with *NGR1$^{-PALM\&PBR2}$* displayed partially compromised restoration of the main root angle upon reorientation, while the *NGR1$^{-PALM\&PBR1\&2}$* root bending was completely disrupted (Fig. 3B). With confocal microscopy we observed the dissociation of the NGR1$^{-PALM\&PBR2}$ and NGR1$^{-PALM\&PBR1\&2}$ from the PM (Fig. 3C). PM/cytoplasm ratio was significantly decreased for both NGR1$^{-PALM\&PBR2}$ and NGR1$^{-PALM\&PBR1\&2}$ compared to non-mutated NGR1-GFP (Fig. 3D). Taken together, the combination of mutations in polybasic regions and palmitoylation site resulted in the decrease of NGR1-GFP PM binding and loss of the protein functionality.

If the selected polybasic regions and palmitoylation site represent solely the mean of the PM anchoring, then bringing the protein back to the PM by different targeting signal should restore its functionality. To test this hypothesis, we introduced another membrane-association site to the mutant versions of NGR1-GFP. It was shown that the N-terminus of LZY1 mediates its membrane localization potentially via a predicted N-myristoylation site (Yoshihara and Spalding, 2020). This site is not conserved in the NGR1. Remarkably, LZY1 does not possess the palmitoylated Cys residue conserved in NGR1 (Fig. S4A). We changed the N-terminus of all the NGR1 mutant versions carrying the mutation $C^{206}A$ to introduce the LZY1 N-terminal myristoylation site. The obtained *NGR1$^{Nmyr\ -PALM}$-GFP, NGR1$^{Nmyr\ -PALM\&PBR2}$-GFP, NGR1$^{Nmyr\ -PALM\&PBR1\&2}$-GFP* versions under *NGR1* native promoter were transformed to the *ngr1/2/3*.

As an alternative, we used a well-characterized membrane-association sequence from the C-terminus of ROP2 (ROP-CT) carrying a polybasic region and geranyl-geranylation site (Fig. S4B) (Lin et al., 1996; Yalovsky et al., 2008). Similarly, as for the N-myristoylation site, we added the ROP-CT on the C-terminus after the GFP tag to all the variants with the mutated PALM site. The resulting *NGR1p::NGR1$^{-PALM\ ROP-CT}$-GFP, NGR1p::NGR1$^{-PALM\&PBR2\ ROP-CT}$-GFP, NGR1p::NGR1$^{-PALM\&PBR1\&2\ ROP-CT}$-GFP* were transformed into *ngr1/2/3* background. PM localization and gravitropic response of the versions with another acylation site were restored gradually (Fig. S4C-H).

We examined the localization of the GFP signal in the columella of both restored lines (*NGR1p::NGR1$^{Nmyr\ -PALM\&PBR1\&2}$-GFP* and *NGR1p::NGR1$^{-PALM\&PBR1\&2\ ROP-CT}$-GFP*). NGR1$^{Nmyr\ -PALM\&PBR1\&2}$ membrane association was partially restored, and NGR1$^{-PALM\&PBR1\&2\ ROP-CT}$

membrane association was fully restored (Fig. 3E,F). In accordance with PM localization, the gravitropic response of those plants was also restored (Fig. 3G,H).

Thus NGR1 PM localization is mediated synergistically by polybasic regions and palmitoylation site, and the NGR1 PM association is crucial for NGR1 functioning in root gravitropic response.

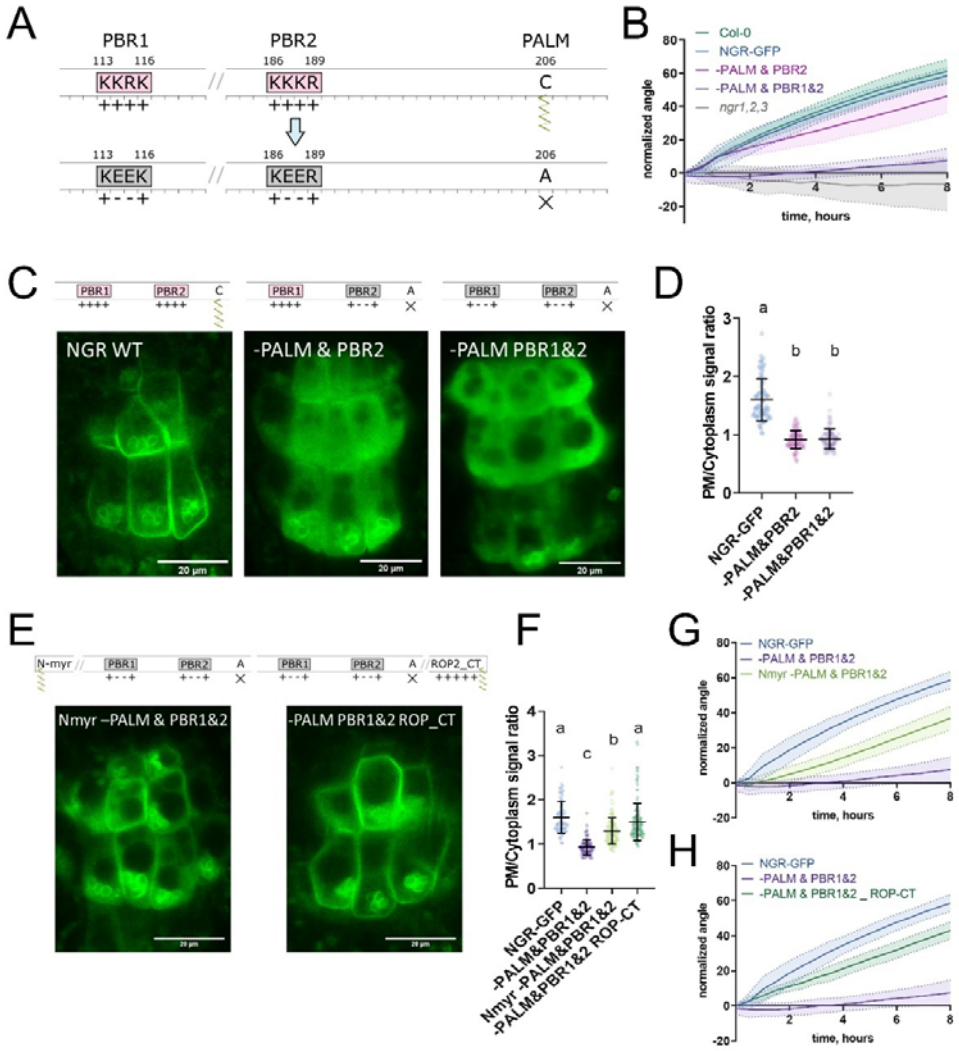

Fig. 3 | Polybasic regions and a palmitoylation site mediate NGR1 membrane localization.

A) Scheme of mutagenesis. K114E&R115E (-PBR1), K187E&K188E (-PBR2), and C206A (-PALM) were introduced to disrupt NGR1 polybasic regions and palmitoylation site. Different combinations of mutations were tested.

B) Main root angle restoration upon reorientation in the vertical scanner setup of the *ngr1/2/3* triple mutant complemented with *NGR1p::NGR1*$^{-PALM\&PBR2}$*-GFP* and

NGR1p::NGR1$^{-PALM\&PBR1\&2}$*-GFP* in comparison to *NGR1p::NGR1*^{WT}*-GFP*, Col-0 and *ngr1/2/3* triple mutant.

C) Representative confocal microscopy images of the root columella cells.

D) PM/cytoplasm signal ratio for NGR1p::NGR1-GFP, NGR1p::NGR1$^{-PALM\&PBR2}$-GFP, and NGR1p::NGR1$^{-PALM\&PBR1\&2}$-GFP variants. Mutation in the polybasic region and palmitoylation site leads to the dissociation of NGR1 protein from the PM. For statistical analysis one-way ANOVA test was used, 'a' is significantly different from 'b' with a p-value<0.0001. The difference between the PM/Cytoplasm signal ratio of NGR1p::NGR1$^{-PALM\&PBR2}$-GFP and NGR1p::NGR1$^{-PALM\&PBR1\&2}$-GFP is not statistically significant.

E) Representative pictures of the root columella cells of *NGR1*$^{Nmyr\ -PALM\&PBR1\&2}$*-GFP* and *NGR1*$^{-PALM\&PBR1\&2\ ROP-CT}$*-GFP*. Membrane localization of NGR1$^{-PALM\&PBR1\&2}$-GFP is restored upon the addition of LZY1 N-terminal myristoylation site (left) or C-terminal region of ROP2 bearing polybasic region and geranyl-geranylation site (right).

F) PM/cytoplasm ratio quantified for the versions with another acylation site. Different letters designate the statistically significant difference with p<0.0001 in a one-way ANOVA test.

G) Rescued main root angle restoration upon reorientation in the vertical scanner setup of the *NGR1p::NGR1*$^{Nmyr\ -PALM\&PBR1\&2}$*-GFP* in *ngr1/2/3* line, after the addition of LZY1 N-myristoylation site to the NGR1 version with mutated polybasic regions and palmitoylation site.

H) Rescued gravitropic response of the *NGR1p::NGR1*$^{-PALM\&PBR1\&2\ \ ROP-CT}$*-GFP* in *ngr1/2/3*, with the addition of the C-terminus of the ROP2 after the GFP tag.

For all the mutant variants more than 5 separate transgenic lines were observed with similar results. 8-15 roots were quantified for each gravitropic bending experiment. Shaded regions depict SD.

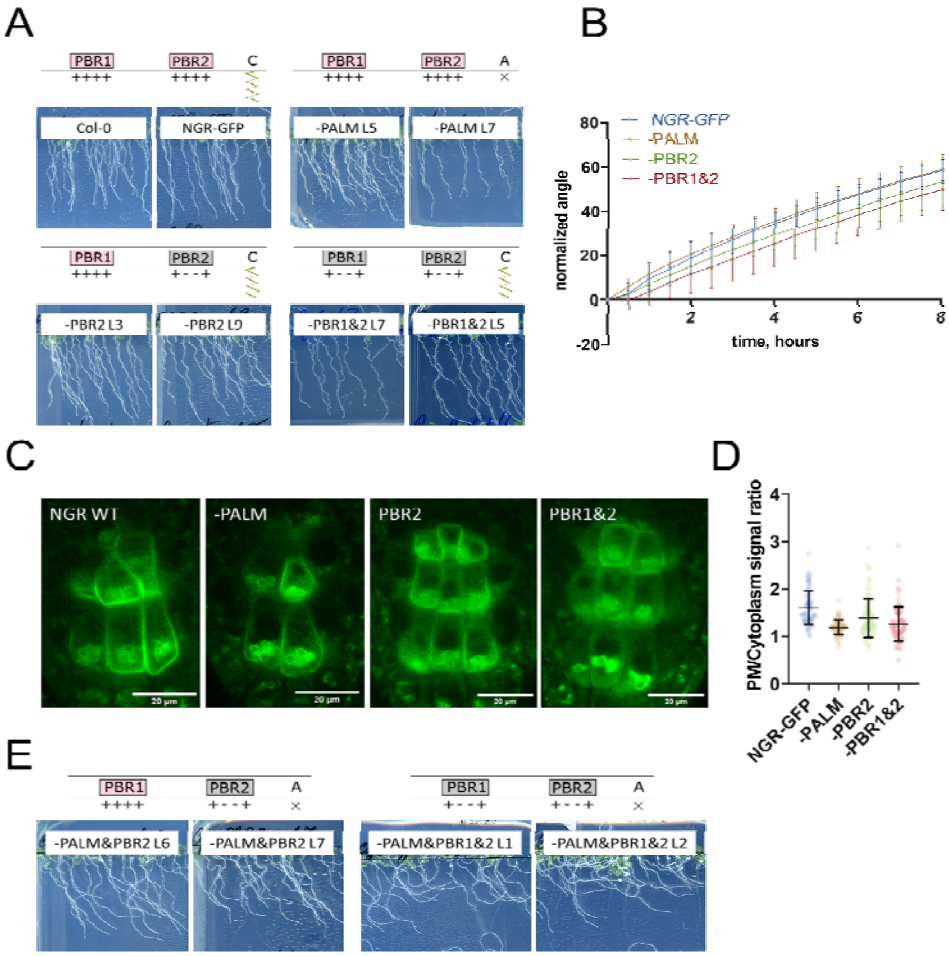

Fig. S3 | Mutations only in PALM site or PBRs are insufficient to disrupt NGR1 function and localization.

A) Phenotypes of the 5 d.o. seedlings of *ngr1/2/3* complemented with *NGR1p::NGR1-GFP*, *NGR1p::NGR1^{-PALM}-GFP*, *NGR1p::NGR1^{-PBR2}-GFP*, *NGR1p::NGR1$^{-PBR1\&2}$-GFP*.

B) Restoration of the main root angle upon reorientation in the vertical scanner setup.

C) Representative pictures of the root columella cells expressing different versions of NGR1p::NGR1^{mut}-GFP.

D) Quantification of the PM/cytoplasm ratio for NGR1p::NGR1^{mut}-GFP variants.

E) Phenotypes of the 5 d.o. seedlings of the *NGR1p::NGR1$^{-PALM\&PBR2}$-GFP* in *ngr1/2/3* and *NGR1p::NGR1$^{-PALM\&PBR1\&2}$-GFP* in *ngr1/2/3*.

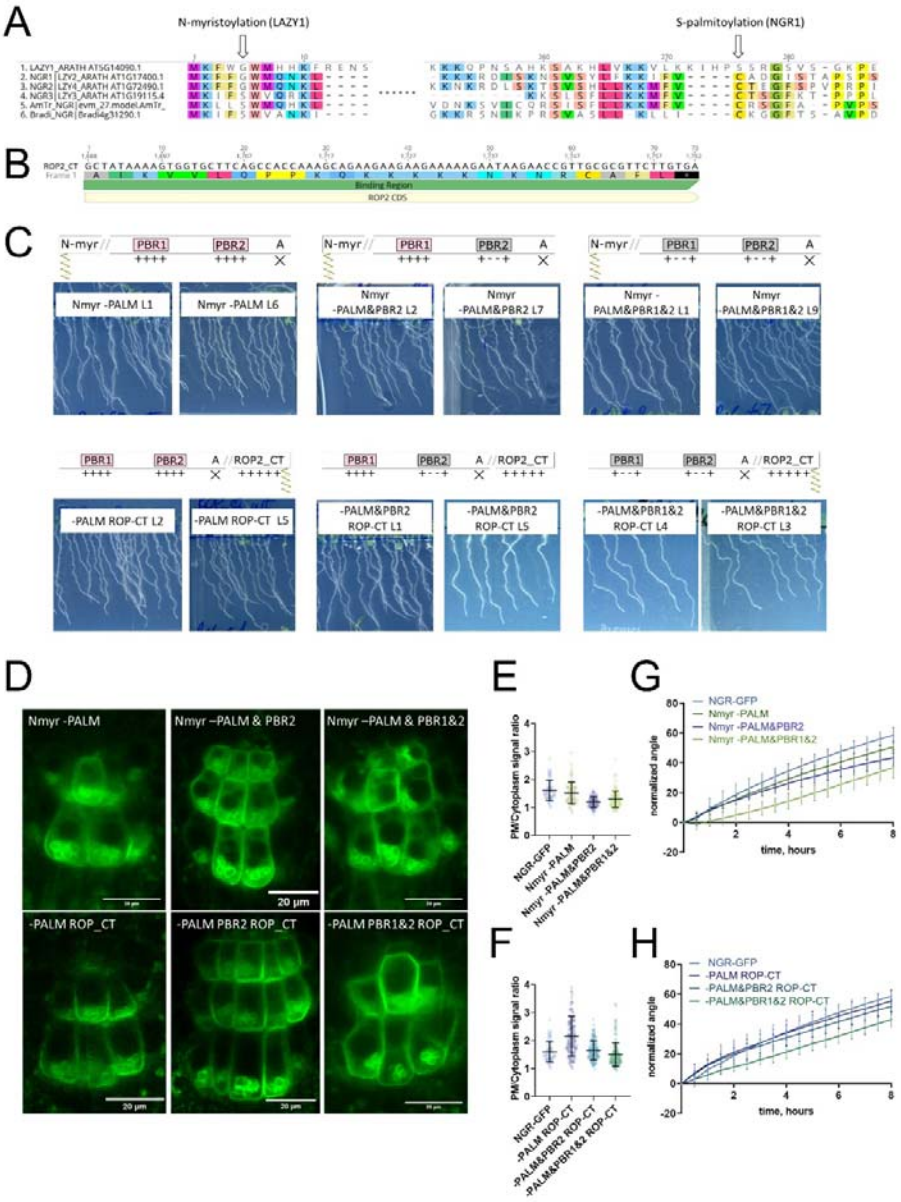

Fig. S4 | Recovery of NGR1^{mut}-GFP function and localization upon addition of another acylation site.

A) Alignment of NGR/LZY homologs. LZY1 has the unique N-terminal myristoylation motif. Palmitoylated Cys conserved in other NGRs is not present in LZY1.

B) The sequence of the ROP2 C-terminus with a polybasic region and geranyl-geranylation site.

C) Phenotypes of the plants. *ngr1/2/3* complemented with different versions of *NGR1p::NGR1^{mut}-GFP* with additional LZY1 N-myristoylation site (upper row) or ROP2 C-terminus under native NGR1 promoter (lower row).

D) Representative pictures of the root columella cells expressing different versions of NGR1p::NGR1^{mut}-GFP with additional LZY1 N-myristoylation site (upper row) or ROP2 C-terminus (lower row).

E) Quantification of the PM/Cyt ratio for NGR1p::NGR1$^{Nmyr\text{-}mut}$-GFP variants.

F) Quantification of the PM/Cyt ratio for NGR1p::NGR1$^{mut\ ROP\text{-}CT}$-GFP variants.

G) Gravitropic response of the *NGR1p::NGR1$^{Nmyr\text{-}mut}$-GFP* in *ngr1/2/3* variants with added N-myristoylation site. The restoration of the main root angle upon reorientation in the vertical scanner setup.

H) Gravitropic response in the vertical scanner setup of *ngr1/2/3* complemented with the *NGR1p::NGR1$^{mut\ ROP\text{-}CT}$-GFP* variants with added ROP2 C-terminus.

For all the mutant variants more than 5 separate transgenic lines were observed with similar results. 8-15 roots were quantified for each gravitropic bending experiment. Error bars depict SD.

D6PK relocalizes in columella following gravistimulation in NGR1-dependent manner

NGR1 protein relocalization occurs simultaneously with statolith sedimentation and is rapidly followed by PIN-dependent asymmetric auxin accumulation at the lower root side. These events, however, precede a visible PIN3 polarization towards the bottom columella cell sides (Fig. 1D-G). Alternatively, we hypothesized that asymmetric PIN activation at this position may precede the PIN polarization there and mediate the early auxin asymmetry. To test this, we analyzed the localization of D6PK, a well-established PIN3 activating kinase (Willige et al., 2013). We monitored D6PK under its native promoter with N-terminal YFP and mCHERRY (mCH) tags. This revealed a highly dynamic polarized D6PK localization following gravistimulation. Following 180° rotation, YFP-D6PK and mCH-D6PK displayed a very clear translocation to the new bottom side of the columella cells (Fig. 4A-C). To resolve whether this polarization depends on NGR proteins, we transformed mCHERRY-D6PK (mCH-D6PK) to both *ngr1/2/3* triple mutants and Col-0 wild type plants. Notably, following gravistimulation, D6PK polarization was absent in *ngr1/2/3* triple mutants (Fig. 5C-D, Supplementary movie 2). Surprisingly, other cell types such as meristematic cells or epidermal cells still displayed undisturbed basal (WT-like) D6PK polarity in *ngr1/2/3* triple mutant suggesting a role of NGRs in D6PK targeting specifically during gravity response (Fig. 4C). To compare D6PK translocation with other events during gravity response, we generated a movie, where polarization of D6PK is compared with the calcium transients, PIN3 mobility, and DII Venus signal (Supplementary movie 3).

Taken together, we identified D6PK, a PIN activating kinase to be translocated towards the bottom columella cell sides in an NGR-dependent manner. This provides a plausible mechanism for rapidly redirecting auxin fluxes prior to PIN relocation during root gravitropic response.

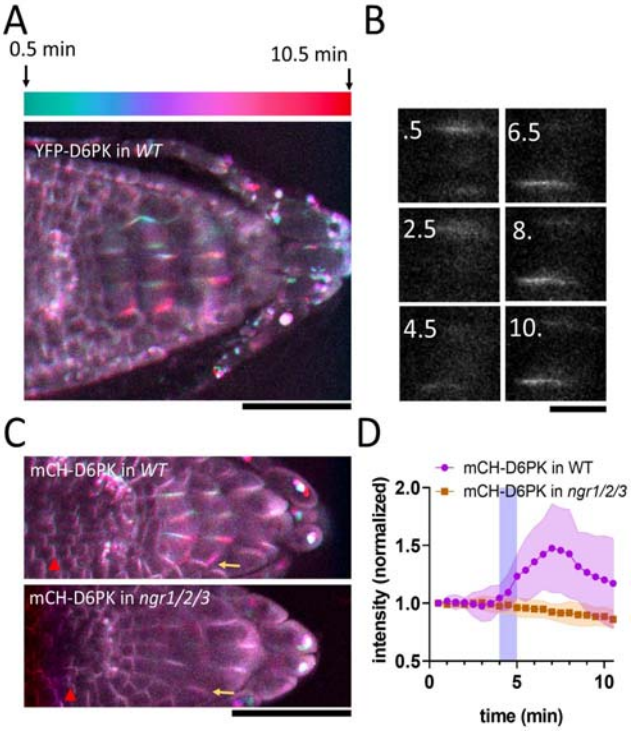

Fig.4 | NGR-Dependent D6 protein kinase translocation.

A) Temporal color-coded image of YFP-D6PK translocation induced by 180° rotation.

B) Single gravistimulated (180°) columella cell undergoing YFP-D6PK translocation. White numbers indicate time after rotation (min).

C) mCH-D6PK 10 min after gravistimulation in WT and *ngr1/2/3* triple mutant, same temporal color code as in A. Yellow arrow depicts the new bottom membrane. Red arrowhead depicts meristematic cells, which displayed basal D6PK polarity in both genotypes.

D) Quantification of D6PK signal at the columella cell bottom PM upon 180° rotation. Blue strip depicts approximate time of statolith contact with the bottom PM.

Bars = 50 µm (A,C) 10 µm (B). 10 cells out of 3 roots were quantified. Experiment was replicated 3 times with similar results. Shaded regions depict SD.

Discussion

In this study, we provide several new crucial insights into the mechanism through which plant roots adapt their growth in response to gravity: (i) we mapped the early events after gravistimulation with unprecedented time resolution challenging the current gravitropic models; (ii) we observed real-time relocalization of the key gravitropic regulator, NGR1 on and alongside the descending statoliths and (iii) mapped the conditions for NGR1 crucial association with the PM; and, finally, (iv) we detected rapid, NGR1-dependent relocation of D6PK auxin transport activator. This altogether suggests a new mechanism for rapid redirection of auxin fluxes following gravistimulation.

Early events during root gravitropic response

The temporal correlation between NGR1 relocation and auxin asymmetry dynamics was tested by monitoring auxin-dependent calcium transients. Interestingly, while an auxin-induced calcium wave can be observed following statolith descent to the bottom side of the gravity-sensing cells, preceding this, a decline in calcium transients occurs at the upper root side. These observations suggest that the first signaling event in root gravitropic bending may not be statolith contact with the cell bottom, but rather the departure of statoliths from the upper PM, closely followed by NGR1 and D6PK translocation to the bottom cell sides. Only significantly later, similar polarization of PIN auxin exporters can be confidently observed. This may be reflected by actual onset of the root bending, as there is growing evidence, that the actual root bending begins much sooner than previously reported, in fact, some degree of bending was observed already within the first 5 minutes following gravistimulation (Dubey et al., 2023; Serre et al., 2023).

Insights into NGR membrane association and gravity-induced polarization

NGR-GFP relocation to the new bottom membrane happens rapidly and is not affected when ARF GEF-mediated endomembrane trafficking is inhibited. Although the precise mechanism of NGR1 dynamic relocation following gravitropic stimulus still remains elusive, this study brings some new insights. The NGR1 membrane anchoring mechanism is dependent on cysteine acylation and adjacent polybasic stretches, which interact with charged lipids at the membrane surface. Such a mechanism is typical for a plethora of proteins (Hemsley and Grierson, 2008). Since we could restore the protein functionality by adding two different membrane anchors on the NGR1 N and C terminus, we conclude that the mechanism of membrane targeting is rather universal. Point mutated NGR1 proteins which lost their membrane binding ability still retained the statolith binding, implying an independent targeting mechanism. Therefore, we can conclude that statolith-bound NGR1 is not sufficient for the NGR1 function in gravitropism. On the other hand, NGR amyloplast

association is apparently an essential aspect of the NGR mobility. While writing this manuscript, two concurrent articles have addressed the mechanism of NGR starch grain association and its translocation to the plasma membrane. These studies reveal that the mobility of the NGR (LAZY4) protein depends on the N-terminal transit peptides. The association of LAZY4 with the translocons in the outer plastid membrane is modulated by mitogen-activated protein kinases, facilitating its dynamic transfer to the plasma membrane (Nishimura et al. 2023; Chen et al. 2023) with a specific lipid composition.

Our pharmacological experiments indicate that both sterols and charged lipids play a role in the NGR membrane binding. This resembles other highly polarized structures such as root hairs, where sterols and phosphatidylinositol 4,5-bisphosphate are vital for the polarity (Champeyroux et al., 2020; Ovecka et al., 2010). Furthermore, PIN2 polarity was defective in sterol synthesis mutants, implying the role of sterols in planar polarity as well (Men et al., 2008). Whether there is mobile sterol-rich domain moving alongside the statolith or the membrane composition is uniform remains to be elucidated.

Gravity-induced D6PK kinase polarization as mechanism for rapid auxin fluxes redirection

PIN auxin transporters were shown to polarize following gravistimulation to the bottom of gravity-sensing cells (Friml et al., 2002; Furutani et al., 2020; Kleine-Vehn et al., 2010) providing a mechanism for redirection of auxin fluxes downwards. Although PIN polarization has been shown to be reliant on NGR proteins (Ge and Chen, 2019), the timing of early gravitropic events resolved here suggests that it occurs too late to account for the initial auxin asymmetry. Either, we are unable to detect early, less-pronounced PIN asymmetry or there is an additional mechanism preceding the auxin flux redirection via PIN relocation.

Our discovery of similar gravity-induced polarization of D6PK AGCVIII kinases, which is contingent on NGR activity, bridges this critical knowledge gap and suggests that, prior to relocation of PIN transporters, AGCVIII-mediated PIN activation at the lower cell sides rapidly redirects auxin fluxes following gravity perception. Notably, PIN3 phosphorylation is important for gravity response (Grones et al., 2018) and higher-order D6PK mutants display mild gravitropic bending phenotypes (Zourelidou et al., 2009), which are, however, weaker than *ngr1/2/3* mutants. This observation might be attributed to the multiplicity of the AGC kinase family and/or an additional mechanism governing the differential accumulation of PIN proteins, following D6PK polarization, thus contributing to the regulation of auxin flux.

Similarly to NGRs, D6PK membrane localization depends on polybasic regions and sterol-rich environments (Barbosa et al., 2016; Stanislas et al., 2015). However, in contrast to NGR proteins, D6PK localization is dependent on BFA-sensitive trafficking regulator GNOM (Barbosa et al., 2016, 2014) and thus is likely delivered to the PM by vesicle trafficking. RLD proteins, implicated in the regulation of the GNOM-dependent PIN trafficking pathway, are directly recruited by NGR homolog NGR3 (LZY3) (Furutani et al., 2020). Notably, RLD proteins contain the BRX domain, which is responsible for the NGR interaction (Furutani et al., 2020). In the different cellular context, BRX protein was shown to be an inhibitor of AGC kinase (PAX) induced PIN3 activation and an interactor of multiple D6PK proteins (Marhava et al., 2018). This implies that BRX containing proteins may act as negative feedback on PIN phosphorylation after gravistimulation. Indeed, our observations indicate that the D6PK signal at the new bottom membrane reaches its maximum approximately 7-8 minutes after gravistimulation and subsequently diminishes, hinting at the existence of a negative feedback mechanism. The involvement of RLDs in this process remains to be investigated.

Taken together, an updated model of early events in root gravity-sensing cells emerges: (i) Statoliths sediment and bring associated NGR proteins to the lower PM; by a mechanism requiring electrostatic interaction-based association of NGR with the PM; (ii) dependent on these events, the D6PK translocates almost concomitantly also to the bottom cell sides, likely by GNOM-dependent trafficking mechanism; (iii) D6PK activates PINs at the lower side, auxin transport get redirected downwards reflected by a decrease of auxin response at the upper side followed by auxin response increase at the lower root side; (iv) D6PK asymmetry gradually diminishes, possibly by action of BRX domain-containing proteins and the whole PIN-dependent auxin transport machinery gradually relocates to the lower cell side for more sustained redirection of auxin fluxes. There are still many mechanistic links to be confirmed and clarified in this model but it is consistent with all observations on the sequence of events following gravistimulation and with all additional data from other developmental contexts.

Materials and methods

Plant cultivation

All Arabidopsis mutants and transgenic lines which were used in this project are in the Columbia-0 (Col-0) background. *NGR1p::NGR1-GFP*, *35Sp::NGR1-GFP*, and *D6PKp::mCH-D6PK* were generated as part of this research project. *D6PKp::YFP-D6PK* has been described previously (Zourelidou et al., 2009). Overnight seed sterilization was

executed with chlorine gas. Seeds were sown on solid agarose media – half-strength Murashige and Skoog (0.5x MS) medium supplemented with 1% sucrose and 0.8% phyto agar (pH=5.9) – stratified at 4°C for 2 days and subsequently grown vertically at 21°C with 16h light/8h dark cycles.

Cloning strategy

NGR1 promoter was amplified from genomic DNA using the primer pairs NGR1p-B4-FP and NGR1p-B1r-RP, and was cloned into pDONR-P4P1r. *NGR1-GFP* fusion fragment was obtained by overlapping PCR using the prime pairs NGR1g-B1-FP and NGR1g-L-RP to amplify the *NGR1* protein-coding region with genomic DNA as the template and the primer pairs eGFP-L-FP and eGFP-B2-RP to amplify the *eGFP* coding sequence, with a PKPA protein linker inserted between NGR1 and GFP, and the resulting fragment was cloned into pDONR221. The resulting pENTRY clones were recombined into pH7m24GW to get the final expression construct *NGR1p::NGR1-GFP*. The pENTR clone NGR1-GFP in pDONR221 was recombined with pH2GW7 to get the construct *35Sp::NGR1-GFP*.

To obtain desired point mutations in polybasic regions and acylation sites, Mutagenesis of *NGR1p::NGR1-GFP* was performed using Gibson assembly (NEB HiFi DNA assembly E2621L), overlapping compatible cohesive ends were modified. For ROP C-terminus, an oligo-bridge Gibson assembly was performed with an oligonucleotide containing the entire ROP2 hypervariable region. Plants were transformed with floral dip method (Zhang et al., 2006).

NGR1 transformants were selected on plates containing 30 µg/ml hygromycin. *NGR1p::NGR1-GFP* plants with genotyped with primers gNGRmut-NGR1prom-fwd and gNGRmut-T35S-rev, and the middle part of the NGR1 was sequenced to confirm the presence of the mutations.

D6PKp::mCH-D6PK was generated using the Greengate cloning strategy. Greengate entry blocks were generated with the use of the Gibson assembly (pGGA-D6PK promotor) and restriction-ligation assembly (pGGC-D6PK). 2KB fragment upstream of D6PK start codon was used and the BsaI site was removed using point mutated compatible cohesive ends for the Gibson assembly between fragments A and B. Other building blocks used were: pGGB-mCHERRY-linker (pGGB001), pGGD-Dummy (pGGD002), pGGE UBQ10 terminator (pGGE009), pGGF-d-AlanineR (pGGF003), destination vector (pGGZ001 modified to contain bacterial kanamycin resistance; Lampropoulos et al., 2013), plasmids were obtained from Addgene or were kindly provided by Dr. Andrea Bleckmann. *pD6PK::mCH-D6PK* transformants bearing DAO-selection cassette were selected on the 3 mM D-Alanine.

Microscopy

For imaging, vertically mounted Zeiss LSM800 was used with air objectives Plan Apochromat 20x/0.8 M27 and Plan Apochromat 10x/0.45 M27 (Fig. 1G). Air objective Plan Apochromat 20x/0.8 M27 and water objective Plan-Apochromat 40x/1.2 M27 were used in Fig. 2 and Fig. S1, S2. Plan apochromat 60x 1.4 Oil objective was used for the airyscan imaging (Fig. S1C). For fluorescence lifetime imaging (Fig. S1B), Leica Stellaris 5 with Plan-Apochromat 40x/1.2 M27 was used. GCaMP signal was imaged using GFP emission (500-540 nm) using 405 nm and 488nm excitation lasers. Signal obtained by 405 nm excitation was used as a ratiometric reference. For the gravitropic experiments, brightfield images were always taken together with the fluorescent probes to determine the statolith contact with basal PM. This was determined as a time at which statolith movement relative to the cell surface stopped.

Plant treatments

The following inhibitors were dissolved in DMSO: Brefeldin A (Sigma); Cycloheximide (Sigma); PAO (Sigma); Fenpropimorph (Sigma); Lovastatin (Sigma); NPA (DUCHEFA N0926). BFA treatment was performed as described previously (Geldner et al., 2001). In brief, seedlings were submerged in liquid MS medium and pre-treated with 50µM CHX for 30 minutes. Subsequently, they were incubated with 50 µM BFA and 50 µM CHX for 75 minutes. Then, 2 µM FM4-64 was added and co-incubated with 50 µM BFA and 50 µM CHX for 15 minutes. Treatment with PAO was executed as described previously (Barbosa et al., 2016); seedlings were incubated in 30 µM PAO-containing liquid MS medium for 20 minutes, followed by the addition of 2 µM FM4-64 and another 10-minute incubation. For quantification purposes, 5-day-old seedlings grown on AM+ plates with 1 µM LOV and 250 µg/ml FEN were utilized (Stanislas et al., 2015). Representative images were captured of 5-day-old seedlings that were initially grown on AM+ and subsequently transferred to 1 µM LOV and 50 µg/ml FEN for a duration of 2 hours. To treat with DTT, seedlings were incubated in liquid MS medium supplemented with 50 mM DTT (Sigma; dissolved in H2O) for 3 hours, followed by a 10-minute incubation with 2 µM FM4-64 (Sabol et al., 2017). Unless otherwise stated, treated seedlings were mounted in liquid MS medium for live imaging. As a control for used inhibitors, solvent control treatments were performed in parallel.

Data analysis

To quantify signals in the individual cells, time series were stabilized by Correct 3D drift Fiji plugin. All image data was obtained in 16-bit format. ROI were selected and measured using Microsoft Excel and GraphPad Prism. Data was normalized so that the first value = 1 (Fig. 1 A,D,F, 4D) or by using reference channel (Fig 1E, 2B)

In order to analyze subcellular colocalization we utilized the tool JACoP (Just Another Co-localization Plugin), that allows for a correlation of pixels of dual-channel images based on Pearson's coefficient (Bolte and Cordelières, 2006).

Gravitropic bending experiments were performed in the vertically oriented scanner setup. 4 d.o. seedlings were transferred to a new solid agarose media plate and aligned so that the roots were straightened. Images obtained with 30 min intervals were registered with the Fiji StackReg plugin (Schindelin et al., 2012). Roots were manually tracked and angle increments were calculated using Microsoft Excel.

For the PM/cytoplasm ratio quantification, the background of the confocal images was subtracted; with the multi-point selection tool 15-50 points on the PM, and 15-50 points in the cytoplasm were selected, and the intensity of the GFP signal was measured.

The location of the PM membrane was confirmed with the FM4-64 staining. The PM region was selected on the bottom side of the cells, as NGR1 is localized polarly. The cytoplasmic region was selected close to the selected membrane region and did not include the region with amyloplasts and the vacuole. For individual cells the averaged PM signal was divided by the averaged cytoplasmic signal. The PM/cytoplasm ratio for the lines is quantified as the average of the PM/cytoplasm ratios for individual cells of this line. If not stated otherwise, all experiments were performed in triplicate. 3 or more independent transgenic lines were always used with similar results. All error bars and shaded areas around average represent SD.

List of primers used in the study

Primer name	**Primer sequence**
Transgenic line preparation	
NGR1p-B4-FP	GGGGACAACTTTGTATAGAAAAGTTGGAAGAGGAGAAGGTGGGAGAGC
NGR1p-B1r-RP	GGGGACTGCTTTTTTGTACAAACTTGTGTTTCTTTTTTTCTGACAATTGACTG
NGR1p-S-F1	ACTAAACAACCCCTTTTGAAACC
NGR1p-S-F2	CAAGATTGAAAAACTATTTGCCCT
NGR1g-B1-FP	GGGGACAAGTTTGTACAAAAAAGCAGGCTCCATGAAGTTCTTCGGGTGGATG
NGR1g-L-RP	CACCATAGCAGGCTTAGGTATCTCGAGAACTATGACTGTAATCA
eGFP-L-FP	GAGATACCTAAGCCTGCTATGGTGAGCAAGGGCGAGGAG
eGFP-B2-RP	GGGGACCACTTTGTACAAGAAAGCTGGGTGCTACTTGTACAGCTCGTCCATGCC

pGGC_D6PK _for	AGAAGTGAAGCTTGGTCTCAGGCTCCATGATGGCTTCAAAAACTCC
pGGC_D6PK_rev	AGGGCGAGAATTCGGTCTCACTGATCAGAAGAAATCAAACTCAAGATA
pGGA_D6PKpromA_for	GTGAAGCTTGGTCTCAACCTCTGTTGAACCATTTCTAAAAAAAC
pGGA_D6PKpromA_rev	GAGAGAGAGTCCCAATAAATCGTTACCTG
pGGA_D6PKpromB_for	ATTTATTGGGACTCTCTCTCTCTCTCTCTC
pGGA_D6PKpromB_rev	CGAGAATTCGGTCTCATGTTTAACACAGAGCAATCTTAAAC
pGGA_backbone_for	AACATGAGACCGAATTCTC
pGGA_backbone_rev	AGGTTGAGACCAAGCTTC
Genotyping	
ngr1-F199G07-GT-FP	GCGCAGACAAAAATCTTCTTG
ngr1-F199G07-GT-RP	TTGGTGGACTCGTTTGCTTAC
FLAG-LB4	CGTGTGCCAGGTGCCCACGGAATAGT
ngr2-SAIL723H11-GT-FP	TTTGGTTTTATGGACCCAACC
ngr2-SAIL723H11-GT-RP	AAGAGCTTTCTTCCTCCGATG
SAIL-LB3	TAGCATCTGAATTTCATAACCAATCTCGATACAC
ngr3-GK479C08-GT-FP	GCAAACAGATTTTCTTCACCAC
ngr3-GK479C08-GT-RP	GCACAAGTGGCTTCAAAACTC
GABI-O8409	ATATTGACCATCATACTCATTGC
gNGRmut-NGR1prom-fwd	GTAGTCAAAGTTTGGAACTTGAACACC
gNGRmut-T35S-rev	CTGGGAACTACTCACACATTATTCTGG
Mutagenesis	
mutatePBR2-fwd	TAAGAATAACAAGGAAGAAAGAGACATAAGCAAGAACTCTG
mutatePBR2-rev	TCTTTCTTCCTTGTTATTCTTACTCTCTATTGATATCTC
PBR1&2-fragment1-bb-fwd	TAAGAATAACAAGGAAGAAAGAGACATAAGCAAGAACTCTG
PBR1&2-fragment1-bb-rev	TCACATCAGACTTTTCTTCCTTAGTTCTTGACAAGAGCTTC
PBR1&2-fragment2-insert-fwd	AAGGAAGAAAAGTCTGATGTGAATAGAGAGC
PBR1&2-fragment2-insert-rev	TCTTTCTTCCTTGTTATTCTTACTCTCTATTGATATCTC
mutatePALM_C206A-fwd	CAAGAAGATTTTTGTCGCTGCAGATGGG
mutatePALM_C206A-rev	CAGCGACAAAAATCTTCTTGAAAAGATATGAGACAGAG
add-Nmyr-fwd	CCACAAGTTCAGGGGGGATCATAACAGAACAAGCACTTCC
add-Nmyr-rev	CCTGAACTTGTGGTGCATCCACCCCCAGAACTTCATGGAGCC
ROP2-CT-oligo-bridge	GCTATAAAAGTGGTGCTTCAGCCACCAAAGCAGAAGAAGAAGAAAAAGAATAAG
NGR-ROP2_CT-after-GFP-fwd	ACCGTTGCGCGTTCTTGTGACACCCAGCTTTCTTGTAC
NGR-ROP2_CT-after-GFP-rev	TGAAGCACCACTTTTATAGCCTTGTACAGCTCGTCCATG

Acknowledgements

The research leading to these results has received funding from the European Research Council (ERC) under the European Union's Horizon 2020 research and innovation programme grant agreement No 742985 and Austrian Science Fund (FWF): I3630-775 B25 to J.F. This research was also supported by the Lab Support Facility (LSF) and the Imaging and Optics Facility (IOF) of IST Austria, namely Tereza Bělinová for her help with the imaging. J.S. was supported by FemTECH fellowship.

References

Abas L, Kolb M, Stadlmann J, Janacek DP, Lukic K, Schwechheimer C, Sazanov LA, Mach L, Friml J, Hammes UZ. 2021. Naphthylphthalamic acid associates with and inhibits PIN auxin transporters. *Proc Natl Acad Sci U S A* **118**. doi:10.1073/pnas.2020857118

Band LR, Wells DM, Larrieu A, Sun J, Middleton AM, French AP, Brunoud G, Sato EM, Wilson MH, Péret B, Oliva M, Swarup R, Sairanen I, Parry G, Ljung K, Beeckman T, Garibaldi JM, Estelle M, Owen MR, Vissenberg K, Hodgman TC, Pridmore TP, King JR, Vernoux T, Bennett MJ. 2012. Root gravitropism is regulated by a transient lateral auxin gradient controlled by a tipping-point mechanism. *Proc Natl Acad Sci U S A* **109**:4668–4673.

Barbosa ICR, Shikata H, Zourelidou M, Heilmann M, Heilmann I, Schwechheimer C. 2016. Phospholipid composition and a polybasic motif determine D6 PROTEIN KINASE polar association with the plasma membrane and tropic responses. *Development* **143**:4687–4700.

Barbosa ICR, Zourelidou M, Willige BC, Weller B, Schwechheimer C. 2014. D6 PROTEIN KINASE activates auxin transport-dependent growth and PIN-FORMED phosphorylation at the plasma membrane. *Dev Cell* **29**:674–685.

Barbosa IC, Schwechheimer C. 2014. Dynamic control of auxin transport-dependent growth by AGCVIII protein kinases. *Curr Opin Plant Biol* **22**:108–115.

Bolte S, Cordelières FP. 2006. A guided tour into subcellular colocalization analysis in light microscopy. *J Microsc* **224**:213–232.

Brunoud G, Wells DM, Oliva M, Larrieu A, Mirabet V, Burrow AH, Beeckman T, Kepinski S, Traas J, Bennett MJ, Vernoux T. 2012. A novel sensor to map auxin response and distribution at high spatio-temporal resolution. *Nature* **482**:103–106.

Champeyroux C, Stoof C, Rodriguez-Villalon A. 2020. Signaling phospholipids in plant development: small couriers determining cell fate. *Curr Opin Plant Biol* **57**:61–71.

Chen J, Yu R, Li N, Deng Z, Zhang X, Zhao Y, Qu C, Yuan Y, Pan Z, Zhou Y, Li K, Wang

J, Chen Z, Wang X, Wang X, He S-N, Dong J, Deng XW, Chen H. 2023. Amyloplast sedimentation repolarizes LAZYs to achieve gravity sensing in plants. Cell 186:4788–4802.e15.

Dubey SM, Han S, Stutzman N, Prigge MJ, Medvecká E, Platre MP, Busch W, Fendrych M, Estelle M. 2023. The AFB1 auxin receptor controls the cytoplasmic auxin response pathway in Arabidopsis thaliana. *Mol Plant* **16**:1120–1130.

Frescatada-Rosa M, Stanislas T, Backues SK, Reichardt I, Men S, Boutté Y, Jürgens G, Moritz T, Bednarek SY, Grebe M. 2014. High lipid order of Arabidopsis cell-plate membranes mediated by sterol and DYNAMIN-RELATED PROTEIN1A function. *Plant J* **80**:745–757.

Friml J, Wiśniewska J, Benková E, Mendgen K, Palme K. 2002. Lateral relocation of auxin efflux regulator PIN3 mediates tropism in Arabidopsis. *Nature* **415**:806–809.

Furutani M, Hirano Y, Nishimura T, Nakamura M, Taniguchi M, Suzuki K, Oshida R, Kondo C, Sun S, Kato K, Fukao Y, Hakoshima T, Morita MT. 2020. Polar recruitment of RLD by LAZY1-like protein during gravity signaling in root branch angle control. *Nat Commun* **11**:76.

Ge L, Chen R. 2019. Negative gravitropic response of roots directs auxin flow to control root gravitropism. *Plant Cell Environ* **42**:2372–2383.

Ge L, Chen R. 2016. Negative gravitropism in plant roots. *Nat Plants* **2**:16155.

Geldner N, Friml J, Stierhof YD, Jürgens G, Palme K. 2001. Auxin transport inhibitors block PIN1 cycling and vesicle trafficking. *Nature* **413**:425–428.

Grones P, Abas M, Hajný J, Jones A, Waidmann S, Kleine-Vehn J, Friml J. 2018. PID/WAG-mediated phosphorylation of the Arabidopsis PIN3 auxin transporter mediates polarity switches during gravitropism. *Sci Rep* **8**:10279.

Hammond GRV, Fischer MJ, Anderson KE, Holdich J, Koteci A, Balla T, Irvine RF. 2012. PI4P and PI(4,5)P2 are essential but independent lipid determinants of membrane identity. *Science* **337**:727–730.

Han H, Adamowski M, Qi L, Alotaibi SS, Friml J. 2021. PIN-mediated polar auxin transport regulations in plant tropic responses. *New Phytol* **232**:510–522.

Hemsley PA, Grierson CS. 2008. Multiple roles for protein palmitoylation in plants. *Trends Plant Sci* **13**:295–302.

Jiao Z, Du H, Chen S, Huang W, Ge L. 2021. LAZY Gene Family in Plant Gravitropism. *Front Plant Sci* **11**:606241.

Kawamoto N, Morita MT. 2022. Gravity sensing and responses in the coordination of the shoot gravitropic setpoint angle. *New Phytol* **236**:1637–1654.

Kiss JZ, Guisinger MM, Miller AJ, Stackhouse KS. 1997. Reduced gravitropism in

hypocotyls of starch-deficient mutants of Arabidopsis. *Plant Cell Physiol* **38**:518–525.

Kiss JZ, Hertel R, Sack FD. 1989. Amyloplasts are necessary for full gravitropic sensitivity in roots of Arabidopsis thaliana. *Planta* **177**:198–206.

Kiss JZ, Wright JB, Caspar T. 1996. Gravitropism in roots of intermediate-starch mutants of Arabidopsis. *Physiol Plant* **97**:237–244.

Kleine-Vehn J, Ding Z, Jones AR, Tasaka M, Morita MT, Friml J. 2010. Gravity-induced PIN transcytosis for polarization of auxin fluxes in gravity-sensing root cells. *Proc Natl Acad Sci U S A* **107**:22344–22349.

Kolesnikov YS, Kretynin SV, Volotovsky ID, Kordyum EL, Ruelland E, Kravets VS. 2016. Molecular mechanisms of gravity perception and signal transduction in plants. *Protoplasma* **253**:987–1004.

Lampropoulos A, Sutikovic Z, Wenzl C, Maegele I, Lohmann JU, Forner J. 2013. GreenGate---a novel, versatile, and efficient cloning system for plant transgenesis. *PLoS One* **8**:e83043.

Lin Y, Wang Y, Zhu JK, Yang Z. 1996. Localization of a Rho GTPase Implies a Role in Tip Growth and Movement of the Generative Cell in Pollen Tubes. *Plant Cell* **8**:293–303.

Li P, Wang Y, Qian Q, Fu Z, Wang M, Zeng D, Li B, Wang X, Li J. 2007. LAZY1 controls rice shoot gravitropism through regulating polar auxin transport. *Cell Res* **17**:402–410.

Marhava P, Bassukas AEL, Zourelidou M, Kolb M, Moret B, Fastner A, Schulze WX, Cattaneo P, Hammes UZ, Schwechheimer C, Hardtke CS. 2018. A molecular rheostat adjusts auxin flux to promote root protophloem differentiation. *Nature* **558**:297–300.

McLaughlin S, Murray D. 2005. Plasma membrane phosphoinositide organization by protein electrostatics. *Nature* **438**:605–611.

Men S, Boutté Y, Ikeda Y, Li X, Palme K, Stierhof Y-D, Hartmann M-A, Moritz T, Grebe M. 2008. Sterol-dependent endocytosis mediates post-cytokinetic acquisition of PIN2 auxin efflux carrier polarity. *Nat Cell Biol* **10**:237–244.

Monshausen GB, Miller ND, Murphy AS, Gilroy S. 2011. Dynamics of auxin-dependent Ca2+ and pH signaling in root growth revealed by integrating high-resolution imaging with automated computer vision-based analysis. *Plant J* **65**:309–318.

Morita MT. 2010. Directional gravity sensing in gravitropism. *Annu Rev Plant Biol* **61**:705–720.

Naramoto S, Otegui MS, Kutsuna N, de Rycke R, Dainobu T, Karampelias M, Fujimoto M, Feraru E, Miki D, Fukuda H, Nakano A, Friml J. 2014. Insights into the localization and function of the membrane trafficking regulator GNOM ARF-GEF at the Golgi

apparatus in Arabidopsis. *Plant Cell* **26**:3062–3076.

Nishimura T, Mori S, Shikata H, Nakamura M, Hashiguchi Y, Abe Y, Hagihara T, Yoshikawa HY, Toyota M, Higaki T, Morita MT. 2023. Cell polarity linked to gravity sensing is generated by LZY translocation from statoliths to the plasma membrane. Science 381:1006–1010.

Ovecka M, Berson T, Beck M, Derksen J, Samaj J, Baluska F, Lichtscheidl IK. 2010. Structural sterols are involved in both the initiation and tip growth of root hairs in Arabidopsis thaliana. *Plant Cell* **22**:2999–3019.

Rakusová H, Gallego-Bartolomé J, Vanstraelen M, Robert HS, Alabadí D, Blázquez MA, Benková E, Friml J. 2011. Polarization of PIN3-dependent auxin transport for hypocotyl gravitropic response in Arabidopsis thaliana. *Plant J* **67**:817–826.

Sabol P, Kulich I, Žárský V. 2017. RIN4 recruits the exocyst subunit EXO70B1 to the plasma membrane. *J Exp Bot* **68**:3253–3265.

Sack FD. 1991. Plant Gravity SensingInternational Review of Cytology, International Review of Cytology. Elsevier. pp. 193–252.

Schindelin J, Arganda-Carreras I, Frise E, Kaynig V, Longair M, Pietzsch T, Preibisch S, Rueden C, Saalfeld S, Schmid B, Tinevez J-Y, White DJ, Hartenstein V, Eliceiri K, Tomancak P, Cardona A. 2012. Fiji: an open-source platform for biological-image analysis. *Nat Methods* **9**:676–682.

Serre NBC, Wernerová D, Vittal P, Dubey SM, Medvecká E, Jelínková A, Petrášek J, Grossmann G, Fendrych M. 2023. The AUX1-AFB1-CNGC14 module establishes a longitudinal root surface pH profile. *Elife* **12**. doi:10.7554/eLife.85193

Stanislas T, Hüser A, Barbosa ICR, Kiefer CS, Brackmann K, Pietra S, Gustavsson A, Zourelidou M, Schwechheimer C, Grebe M. 2015. Arabidopsis D6PK is a lipid domain-dependent mediator of root epidermal planar polarity. *Nat Plants* **1**:15162.

Takahashi K, Takahashi H, Furuichi T, Toyota M, Furutani-Seiki M, Kobayashi T, Watanabe-Takano H, Shinohara M, Numaga-Tomita T, Sakaue-Sawano A, Miyawaki A, Naruse K. 2021. Gravity sensing in plant and animal cells. *NPJ Microgravity* **7**:2.

Taniguchi M, Furutani M, Nishimura T, Nakamura M, Fushita T, Iijima K, Baba K, Tanaka H, Toyota M, Tasaka M, Morita MT. 2017. The Arabidopsis LAZY1 Family Plays a Key Role in Gravity Signaling within Statocytes and in Branch Angle Control of Roots and Shoots. *Plant Cell* **29**:1984–1999.

Vermeer JEM, Thole JM, Goedhart J, Nielsen E, Munnik T, Gadella TWJ Jr. 2009. Imaging phosphatidylinositol 4-phosphate dynamics in living plant cells. *Plant J* **57**:356–372.

Wang L, Li D, Yang K, Guo X, Bian C, Nishimura T, Le J, Morita MT, Bergmann DC, Dong

J. 2022. Connected function of PRAF/RLD and GNOM in membrane trafficking controls intrinsic cell polarity in plants. *Nat Commun* **13**:7.

Willige BC, Ahlers S, Zourelidou M, Barbosa ICR, Demarsy E, Trevisan M, Davis PA, Roelfsema MRG, Hangarter R, Fankhauser C, Schwechheimer C. 2013. D6PK AGCVIII kinases are required for auxin transport and phototropic hypocotyl bending in Arabidopsis. *Plant Cell* **25**:1674–1688.

Xie Y, Zheng Y, Li H, Luo X, He Z, Cao S, Shi Y, Zhao Q, Xue Y, Zuo Z, Ren J. 2016. GPS-Lipid: a robust tool for the prediction of multiple lipid modification sites. *Sci Rep* **6**:28249.

Yalovsky S, Bloch D, Sorek N, Kost B. 2008. Regulation of membrane trafficking, cytoskeleton dynamics, and cell polarity by ROP/RAC GTPases. *Plant Physiol* **147**:1527–1543.

Yoshihara T, Iino M. 2007. Identification of the gravitropism-related rice gene LAZY1 and elucidation of LAZY1-dependent and -independent gravity signaling pathways. *Plant Cell Physiol* **48**:678–688.

Yoshihara T, Spalding EP. 2020. Switching the Direction of Stem Gravitropism by Altering Two Amino Acids in AtLAZY1. *Plant Physiol* **182**:1039–1051.

Yoshihara T, Spalding EP, Iino M. 2013. AtLAZY1 is a signaling component required for gravitropism of the Arabidopsis thaliana inflorescence. *Plant J* **74**:267–279.

Zariwala HA, Borghuis BG, Hoogland TM, Madisen L, Tian L, De Zeeuw CI, Zeng H, Looger LL, Svoboda K, Chen T-W. 2012. A Cre-dependent GCaMP3 reporter mouse for neuronal imaging in vivo. *J Neurosci* **32**:3131–3141.

Zhang X, Henriques R, Lin S-S, Niu Q-W, Chua N-H. 2006. Agrobacterium-mediated transformation of Arabidopsis thaliana using the floral dip method. *Nat Protoc* **1**:641–646.

Zourelidou M, Müller I, Willige BC, Nill C, Jikumaru Y, Li H, Schwechheimer C. 2009. The polarly localized D6 PROTEIN KINASE is required for efficient auxin transport in Arabidopsis thaliana. *Development* **136**:627–636.